EasyChair Preprint

№ 2379

Numerical Anslysis of Cropped Delta Wing with Reflex Camber Cross-Section at Transonic Speed with Leading-Edge Tubercles

Fahad Butt, Imran Akhtar, Tariq Talha and Zafar Bangash

January 13, 2020

Numerical Anslysis of Cropped Delta Wing with Reflex Camber Cross-Section at Transonic Speed with Leading-Edge Tubercles

Fahad Rafi Butt, Dr. Imran Akhtar
Analytics & Computing of Energy Systems
Digital Pakistan Lab, NCBC
Islamabad, Pakistan

Dr. Tariq Talha, Dr. Zafar Bangash
Mechanical Engineering Department
College of Electrical and Mechanical Engineering, NUST
Islamabad, Pakistan

***Abstract*— Most of the modifications in flow control surfaces are bioinspired resulting in enhanced lift and thrust efficiency. In nature, hump back whales have evolved with tubercles at the leading-edge (L.E.) of their flippers. There is a strong evidence from the published literature that leading-edge tubercles (L.E.T.) improve stall characteristics of various lifting surfaces. L.E.T. are also known to reduce flow in the span-wise direction. The reduction in size and vorticity of the wingtip vortices is also a known benefit of adding tubercles at the L.E. of lifting surfaces. In this paper, the effects of L.E.T. are analyzed on a cropped delta wing having reflex camber cross-section (C.S.) at low angle of attack (A.O.A.) and transonic flight speed. An improved performance of the wing with L.E.T. is indicated by the results from the numerical simulations when compared to the baseline design. The improved characteristics of the modified wing (M.W.) in comparison with the baseline wing (B.W.) can be attributed, partly to the varying span-wise pressure distribution near the L.E. of the M.W. The improved performance of the M.W. can also be credited to the creation of a pair of chord-wise vortices behind the tubercle troughs as well as an improved stall performance and reduction in both the strength of wingtip vortices and span-wise flow.**

Keywords—Biomimicry; Tubercles; Transonic; Reflex Camber; Delta Wing

I. INTRODUCTION

Researchers are increasingly looking for inspiration from birds and fish for efficient locomotion. Flapping provides the basis for the lift and thrust forces enabling flying and swimming. Several passive control techniques can be learnt from nature to modify the control surfaces for increased lift and thrust. Similar concepts can be applied at various flow regimes to gain advantage in the overall efficiency of the wing [1-3].

The addition L.E.T. on various lifting surfaces such as wings [4-14], aeronautical/marine propellers [15-18], wind/marine turbines [19-23], axial fans [24] and compressors [25] is known to improve efficiency of the said lifting surfaces. In nature, humpback whales are known to have the L.E.T. on their flippers, as shown in Fig. 1. Tubercles are known to delay stall (w.r.t. A.O.A.), reduce both span-wise flow, size and vorticity magnitude of the wingtip-vortices.

Fig. 1. L.E.T. on the flipper of humpback whale.

The addition of tubercles at the L.E. of the wings increase lift-to-drag ratio (L/D) of the modified[1] wing in comparison with the B.W. [4]. In this study, an increment of 17.6% was noted in the L/D for the M.W. as compared to the B.W. The noted increase in performance of the wing at higher A.O.A. was without any penalty at lower A.O.A. Stealth characteristics of the wings could also be improved due to the reduced wingtip vorticity as a direct result of addition of tubercle to the L.E. of the wing.

The analogy between the L.E.T. and conventional vortex generators was experimentally shown by [8]. The experiments were conducted on two wings. The wings had C.S. of NACA five and four series airfoils i.e. 65-021 and 0021. The important findings from the study are mentioned in the following part of this paragraph. The study concluded that the impact of L.E.T. on L/D ratio of a wing depends on the C.S. of the said wing. This can be said because the aerodynamic efficiency of the wing having NACA 65-021 C.S. was altered more noticeably as compared to the wing with NACA 0021 airfoil employed as the C.S. The tubercles having comparable amplitude-to-

[1] A mention of M.W. or propeller or any lifting surface, refers to a lifting surface with the tubercles at the L.E.

wavelength ratios demonstrated similar fluid flow patterns. In post-stall flow conditions, the tubercles with larger amplitude were more effective. Meanwhile, the tubercles with smaller wavelength improved stall angle and the maximum lift co-efficient of the M.W. as compared to the B.W.

The existence of the counter-rotating chordwise vortices (C.R.C.V.) behind the valleys of tubercles as predicted by [4] was confirmed for low Reynolds number of fluid flow [10]. The focus of this study was a scalloped flipper. A reduction in the span-wise flow was also noted in this study. It was concluded that the C.R.C.V. are a primary reason for the re-energized boundary layer which is present only in the flipper with tubercles at the L.E. The re-energized boundary layer results in the improved performance for the modified flipper at high A.O.A. leading to a delay in stall A.O.A.

A recently published numerical study [15] featured a modified aeronautic propeller. The study showed an improved propeller efficiency for the modified propeller when compared to the reference propeller at a wide range of flight conditions. As a part of this study, the effect of L.E.T. geometry was among the parameters analyzed. It was concluded that propeller with larger amplitude and smaller wavelength tubercles had the most increase in the propeller efficiency. A negligible unsteadiness was noticed in the modified propellers in comparison with the baseline propellers. An average improvement in the efficiency of 14.21% was reported.

Humpback whale flippers were analyzed experimentally at various A.O.A. [11]. An improvement in the L/D was noted for various A.O.A. [11]. Quantitatively, an increment of 40% was reported the in the stall angle. As was the case with previously published research [8], the similarity of tubercles with conventional vortex generators was also noted in this study [11].

A National Renewable Energy Laboratory (NREL) Phase VI wind turbine was analyzed by using computational fluid dynamics [20-21]. A total of twenty different cases were generated and simulated at various tip-speed-ratios. An increase in the shaft torque for the simulated cases above the design point of the turbine was noticed [20]. In terms of annual energy production, it was also noted that the configuration in which tubercles are placed from 95% of the blade span to the blade tip show a 10% improvement in the annual energy production.

As was the case in a previously mentioned study [15], a numerical study on a NREL Phase VI wind turbine [23] also found that the transient and steady-state results for the respective numerical simulations, *with and without tubercles*, were in close agreement with each other. It was also concluded that the modified turbine outperformed the baseline turbine at higher wind speeds.

An experimental study [24] was conducted to study the effect of L.E.T. and fan-blade skew on the axial fan performance. The fan blades with L.E.T. showed lower sound emission and higher efficiency when compared with the axial fans without L.E.T. at same operating conditions. It was also noted that a maximum reduction in fan noise was achieved in the configuration with higher amplitude-to-wavelength ratio i.e. larger tubercle amplitude and smaller tubercle wavelength.

A compressor cascade was analyzed experimentally and the results demonstrate that the total pressure loss can be reduced in the post-stall region. The reduced pressure loss leads to an improvement in the compressor efficiency for the compressor having tubercles at the L.E. [25]. The large-scale flow separation zones present in the baseline compressors were shown to have been clearly transformed into several small sized separation zones in the modified compressors. This study also confirmed the analogy of tubercles with vortex generators.

In the present study, the effect of L.E.T. on cropped delta wing having reflex camber airfoil C.S. was analyzed. Airfoils having reflex camber are a common choice when it comes to flying wing and blended body wing types of aircraft. The manuscript is organized as follows. Section II presents details of the numerical scheme, boundary conditions, validation and verification of the algorithm. Results obtained from the numerical simulations are discussed in detail in Section III.

II. Numerical Methodology

Flow Simulation Premium code [26] is used to simulate steady flow over the wings. The turbulence model, numerical schemes and solver employed are mentioned in the proceeding parts of this paragraph. $\kappa - \varepsilon$ turbulence model is employed with Two-Scales Wall Function approach. Second-order upwinding is used to discretize the acceleration terms. The diffusive terms, *internal stress*, are discretized using central differencing. SIMPLE-R is the solution algorithm for pressure-velocity coupling. The Navier–Stokes equations are mathematically represented as follows:

$$\frac{\partial \rho}{\partial t} + \frac{\partial (\rho \boldsymbol{u}_i)}{\partial \boldsymbol{x}_i} = 0$$

$$\frac{\partial (\rho \boldsymbol{u}_i)}{\partial t} + \frac{\partial (\rho \boldsymbol{u}_i \boldsymbol{u}_j)}{\partial \boldsymbol{x}_j} + \frac{\partial p}{\partial \boldsymbol{x}_i} = \frac{\partial (\tau_{ij} + \tau_{ij}^R)}{\partial x_j} + S_i$$

$$\frac{\partial (\rho H)}{\partial t} + \frac{\partial (\rho \boldsymbol{u}_i H)}{\partial \boldsymbol{x}_i} = \frac{\partial (\boldsymbol{u}_j (\tau_{ij} + \tau_{ij}^R) + q_i)}{\partial \boldsymbol{x}_i} + \frac{\partial p}{\partial t} - \tau_{ij}^R \frac{\partial \boldsymbol{u}_i}{\partial \boldsymbol{x}_j} + \rho \varepsilon + S_i \boldsymbol{u}_i + Q_H$$

where, S_i is a mass-distributed external force per unit mass. The mass-distributed external force per unit mass is summation of porous media resistance represented by S_i^{porous}, a buoyancy $S_i^{gravity} = -\rho g_I$ is the gravitational acceleration component along the i-th coordinate direction and the coordinate system's rotation $S_i^{rotation}$, i.e., $S_i = S_i^{porous} + S_i^{gravity} + S_i^{rotation}$. The subscripts are used to denote summation over the three Cartesian coordinate directions [26].

A. Mesh and Computational Domain

The discretization of the computational domain is completed using a cartesian grid with immersed boundary method. Various advantages of using a combination of cartesian computational mesh and the immersed boundary method are as follows. The solution converges faster, the mesh is very quick to generate, the mesh distortion is very low, has very high-quality elements and the numerical errors are relatively lower. The computational domain employed as well as the mesh is shown in Fig. 2. Manual mesh refinement is performed refine the computational mesh in the area of interest

i.e. around the wing surface, and in the regions of the wake to accurately capture the flow parameters. The computational domain is cubic in shape with each side being ten times the wing-span of the simulated wing. A large enough computational domain ensures that the walls of the computational domain have no interference with the flow around the wing.

B. Boundary Conditions

The simulated conditions have a freestream Mach number in the transonic flow regime i.e. 0.8395 at 101325 Pa and 293.2 K imposed at the fluid inlet (indicated by the single-headed Red arrows in Fig. 3) [27-28]. The fluid outlet has a boundary condition of environment pressure (indicated by the double-headed Blue arrows in Fig. 3). The computational domain walls have a slip boundary condition (indicated by Red squares in Fig. 3) so that the formation of boundary layer at the walls of the computational domain does not interfere with the simulation results. By default, the no-slip condition is applied at the wing surface. The applied boundary conditions result in a free stream fluid velocity of 288.42 $m.s^{-1}$ and a free stream density of 1.203 $Kg.m^{-3}$. An A.O.A. of 3.06° is applied on the wing.

C. Wing Geometries

The computer-aided design (CAD) geometry of the wings is modeled in SolidWorks CAD package, as shown in Fig. 4.

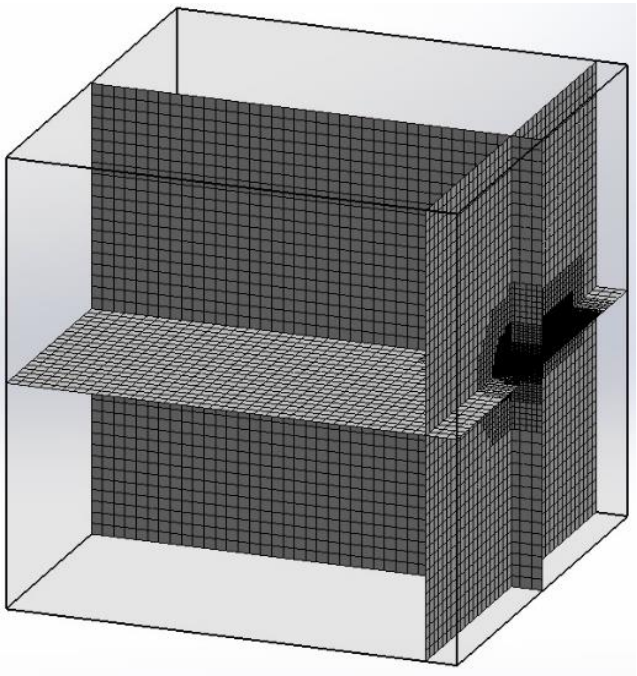

Fig. 2. Mesh and computational domain.

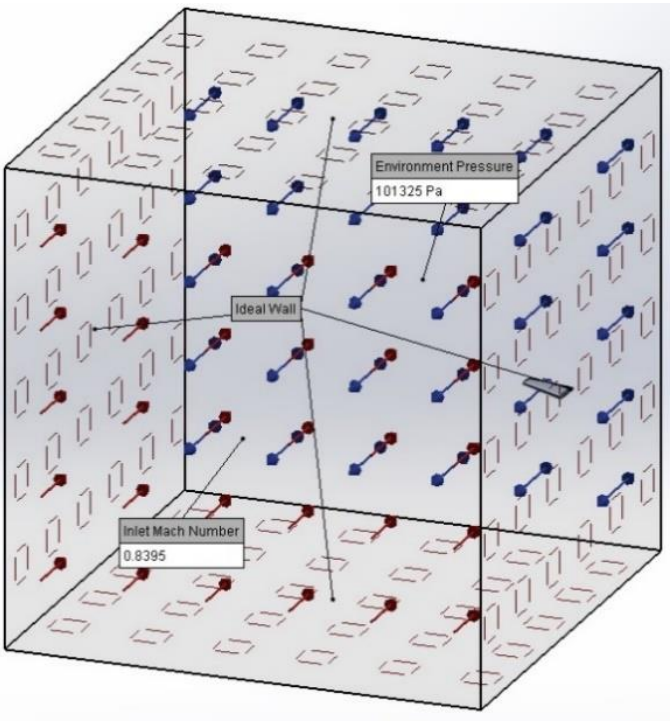

Fig. 3. Boundary conditions.

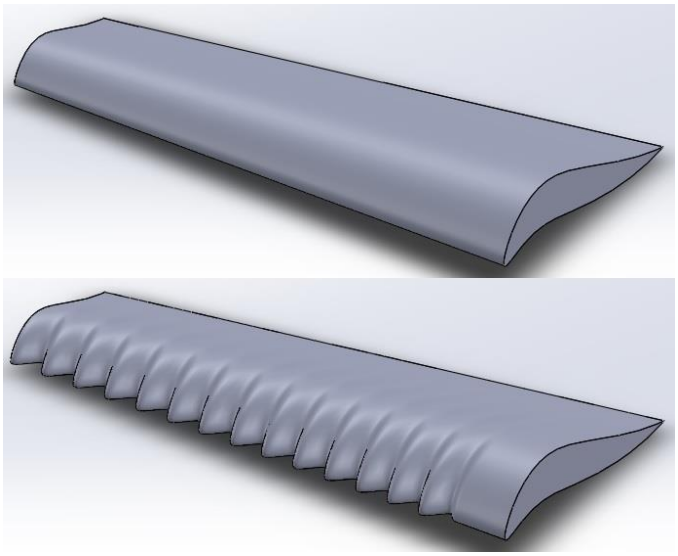

Fig. 4. Wing geometries; T-B, B.W., M.W.

D. Verification and Validation

To validate the computational fluid dynamics analysis, the flow is simulated around an ONERA M-6 wing, as shown in Fig. 5. The ONERA M-6 wing has a C.S. of the ONERA D airfoil.

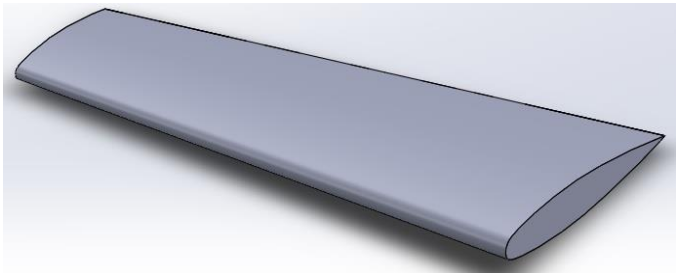

Fig. 5. Wing geometry (ONERA D airfoil C.S.)

It is noted that the results of the numerical simulations are within 8.11% of the results reported by [27-28]. The lift coefficient of the original ONERA M-6 wing is within 3.37 %, meanwhile, the drag coefficient is within 12.85% of the results from the numerical analysis [27-28]. A comparison of the coefficient of pressure between experimental data [27-28] and the present simulation at various span-wise location is shown in Fig. 6.

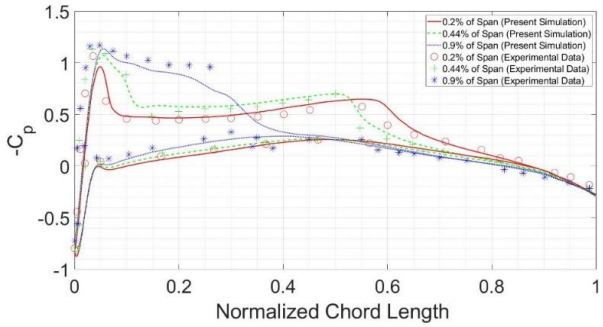

Fig. 6. Surface C_p comparison at various span-wise locations.

a) Grid Refinemet Test

A grid convergence test is performed to make sure that the results obtained from the numerical analysis depended solely on the boundary conditions and not on the mesh cell size. The results from the test are shown in Table I. It is clear from Table I that the results of the mesh M3-M5 are in close proximity to each other, both in terms of forces and moments. Therefore, the mesh setup used for the mesh M3 is selected for this study. The results of the simulations from the present study are compared with [27-28].

TABLE I. MESH INDEPENDENCE TEST RESULTS

Mesh Name	Mesh Cells	Lift [N]	Drag [N]	Moment [N.m]
M1	281,697	9,243.786	977.988	2,176.334
M2	651,190	9,802.965	864.991	2,190.372
M3	2,440,048	10,252.262	861.233	2216.431
M4	3,362,189	10229.222	850.741	2232.391
M5	4,820,709	10141.275	839.721	2241.634

III. RESULTS AND DISCUSSIONS

The L/D of the M.W. is observed to be 12.75% more in compassion with the B.W. design. The calculated L/D for the wing with L.E.T. is 2.98, while the L/D of the wing without L.E.T. came out to be 2.6. By using post processing tools, the flow fields around the baseline ONERA M-6 wing with NACA 55110 C.S. and the modified ONERA M-6 wing with NACA 55110 [2] C.S. and L.E.T. are compared. Following major differences in flow field are observed.

A. Non-Uniform Span-wise Pressure Distribution and Formation of the Counter-Rotating Chord-wise Vorteces

A comparison of the surface pressure distribution is made between the B.W. and the M.W. in Figs. 7-9. The comparison is made with the help of surface plots on the wing, pressure coefficients and C.S. at 56% and 53% of the wing-span. It is to be noted that the location corresponding to 56% of the blade span represents the position of the tubercle trough in the M.W. while the location corresponding to 53% of the blade span represents the position of the adjoining tubercle crest in the M.W.

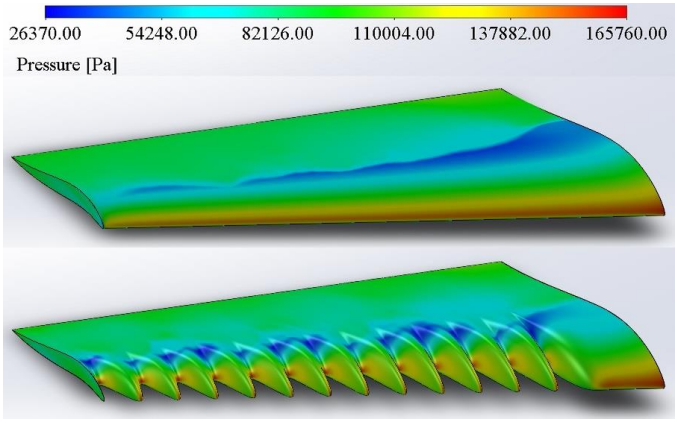

Fig. 7. T-B; B.W., M.W..

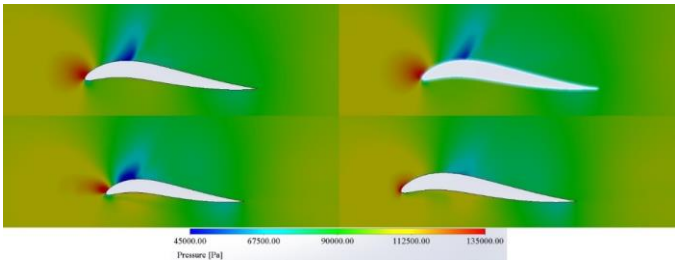

Fig. 8. Top Row, L-R; B.W. C.S. at 56% and 53% of the wing-span; Bottom Row, L-R M.W. C.S. at 56% (tubercle-trough) and 53% (tubercle-crest) of the wing-span.

The pressure on both sides of a wing decreases then increases in the chord-wise orientation, as shown in Figs. 7 and 8. The stagnation region is visible near the L.E. of the wing as the region with higher pressures, which in the wing without the L.E.T. is fairly uniform, as shown in Figs. 7-9. This trend of pressure distribution is present along the entire wing-span of the wing without the L.E.T. The plots for negative coefficient of pressure for B.W. within Fig. 9 also indicate a similar trend.

The irregularity introduced in the stagnation region in the M.W. due to the introduction of L.E.T. is clearly visible in

[2] Any mention of the B.W. employs ONERA M-6 wing with NACA 55110 C.S. Furthermore, any mention of the M.W. employs ONERA M-6 wing with NACA 55110 C.S. and L.E.T.

Figs. 7-9. The shifting of the regions of low pressures in the direction of the L.E. in the wake of tubercle troughs on the suction, *low pressure*, side of the altered wing is clear from Figs. 7-8, in comparison with the tubercle crests. A similar trend of irregular pressure distribution in the span-wise orientation is also noticed on the pressure side of the M.W. However, on the pressure side of the M.W., the high-pressure region seems to shift in the direction of the L.E. in the regions lying behind tubercle troughs when compared with the distribution of pressure in the wake of tubercle crests. As the only difference in the M.W. and the B.W. is the addition of tubercle at the L.E., therefore it can be said that this alternating non-uniform pressure distribution on the M.W. surface is a direct result of addition of the tubercle to the wing geometry. The similar trends are also reported in [4, 8-9,14-16, 21].

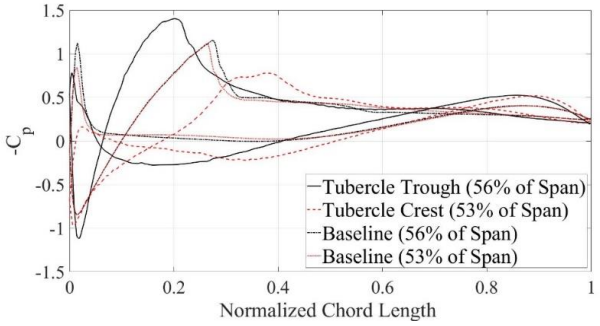

Fig. 9. Surface Coefficient of pressure comparison at different span-wise locations.

The air that passes over a delta wing gets broken down in to two components because of the sweep angle i.e. the span-wise flow and the chordwise flow. The span-wise flow is the component of the flow that is responsible for the creation of a vortex. As air passes over the tubercle, because of the reason mentioned earlier in the paragraph, a vortex is formed on each side of the tubercle. Tubercles can be considered as a set of delta wings arranged in a pattern. It is because of this arrangement that there are two vortices between each peak of the tubercle, each rotating in opposite orientation hence referred to as the counter-rotating vortices, as evident from Fig. 10. These vortices are refereed as C.R.C.V. because these vortices travel in the direction parallel to the wing chord. It can be seen from Fig. 10 that these vortices loose energy, *vorticity*, and gain size, *diameter*, in the chordwise direction. The absence of these vortices from the B.W. is evident as well, in Fig. 10. These trends are also reported by [6, 8-10, 13-15, 24, 26]. It should be noted that in the M.W., the flow remains attached behind the tubercle crests which is not the case in the B.W.

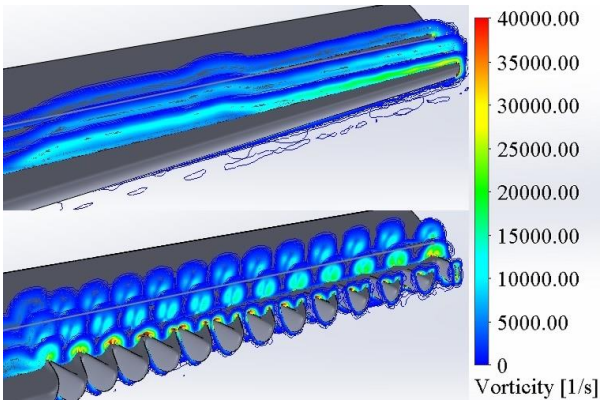

Fig. 10. T-B; B.W., M.W.

B. Delayed Stall, Reduced Wingtip Vortices and Reduced Span-wise Flow

The formation of the high energy C.R.C.V. is responsible for the increased boundary layer momentum in the M.W. which is lost in the B.W. under the same flight conditions. It is evident from Fig. 11 that the attached flow is present on wing surface significantly closer to the trailing edge in the M.W. as compared to the B.W. at the same locations along the wing-span. This observation is also reported by [6, 10-12, 15, 20, 22, 26].

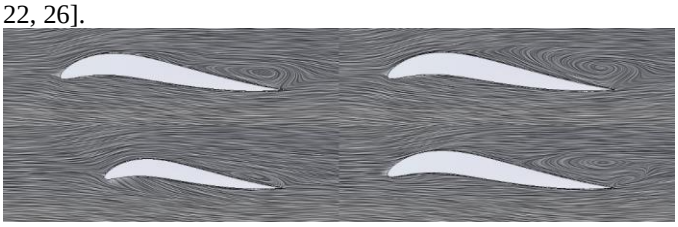

Fig. 11. Top Row, L-R; B.W. C.S. at 56% and 53% of the wing-span; Bottom Row, L-R M.W. C.S. at 56% (tubercle-trough) and 53% (tubercle-crest) of the wing-span.

Wingtip vorticity between the two wings analyzed in the present study is compared using surface plots directly behind the wingtips. The distance at which the circular regions are located is equal to half of the length of the chord at the wingtips. Curl of the velocity field i.e. vorticity magnitude, is used to color the two circular regions within Fig. 12. It can be seen from Fig. 12 that the magnitude of the vorticity is significantly more for the B.W. as compared with the M.W. It is also clear from Fig. 12 that the size of the regions with vorticity of order 4,000 s^{-1} or more is considerably less for the M.W. as compared to the B.W. In the B.W., all of the flow in the span-wise direction is due to the fluid flow from the root to the tip of the wing which results in larger and stronger wingtip vortices. However, the span-wise flow in the M.W. is only due to the tubercle near the wingtip. This is because the C.R.C.V. act as a virtual wing fence. As explained in the paragraphs that follow, span-wise flow is reduced. These observations are also reported by [15, 19, 24].

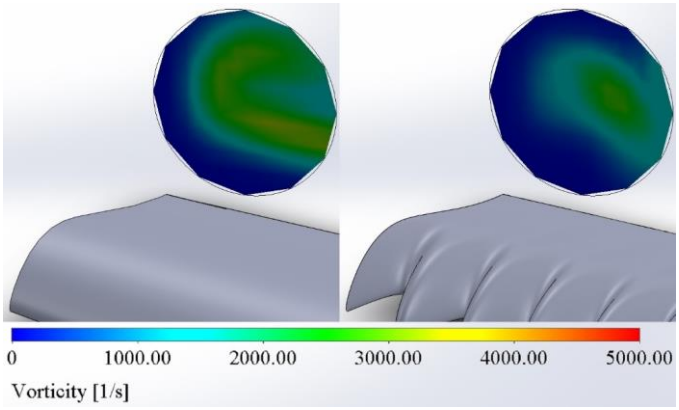

Fig. 12. L-R; B.W., M.W.

Flow trajectories are drawn in Fig. 13 to visualize and compare the magnitude of the span-wise flow between the two wings geometries subject of the analysis in the present study. It can be observed from Fig. 13 that in the M.W., most of the flow is directed in the along the freestream flow also referred to as the chordwise flow because in the present study, the orientation of freestream flow and the wing chord is same. It can also be seen from Fig. 13 that a larger percentage the flow around the B.W. directed towards the span-wise direction. The effect of the C.R.C.V. generated as a result of incorporating tubercles at the L.E. of the wing analogues to a wing fence is also visible in Fig. 13. This observation is also reported by [10, 15].

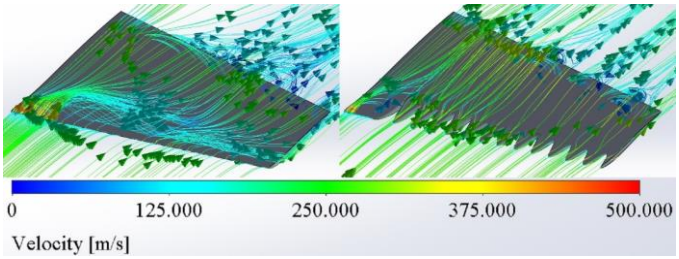

Fig. 13. L-R; B.W., M.W.

IV. Conclusions and Future Work

The efficiency of the cropped delta wing with reflex camber C.S. at transonic flight speed was compared with a modified version of the same wing at same flight conditions. The modification includes the addition of L.E.T. in to the wing geometry. An improved performance of the M.W. is noticed in terms of L/D as compared to the B.W. In the future, the flow field will be analyzed at various A.O.A. as well as the effect of tubercle geometry on the flow field would also be analyzed.

Acknowledgment

This work was conducted with the support of Digital Pakistan Lab established under the National Center for Big Data & Cloud Computing, Pakistan.

References

[1] Akhtar, I., Mittal, R., Lauder, G.V., Drucker, E., “Hydrodynamics of a biologically inspired tandem flapping foil configuration”, Theoretical and Computational Fluid Dynamics, Volume 21, Issue 3, 2007, pp 155–170. https://doi.org/10.1007/s00162-007-0045-2

[2] Khalid, M.S.U., Akhtar, I., Imtiaz, H., Dong, H., Wu, B.., “On the hydrodynamics and nonlinear interaction between fish in tandem configuration”. Ocean Engineering, Volume 157, 2018, pp. 108-120. https://doi.org/10.1016/j.oceaneng.2018.03.049

[3] Khalid, M.S.U., Akhtar, I., Wu, B., “Quantification of flow noise produced by an oscillating hydrofoil. Ocean Engineering”, Volume 171, 2019, pp. 377-390. https://doi.org/10.1016/j.oceaneng.2018.11.024

[4] Watts, P., and Fish, F. E., “The Influence of Passive, Leading Edge Tubercles on Wing Performance,” Proceedings of Unmanned Untethered Submersible Technology (UUST), Autonomous Undersea Systems Inst., Lee, New Hampshire, Aug. 2001.

[5] Fish, F. E., and Lauder, G. V., “Passive and Active Flow Control by Swimming Fishes and Mammals,” Annual Review of Fluid Mechanics, Vol. 38, 2006, pp. 193–224. doi:10.1146/annurev.fluid.38.050304.092201

[6] Rocha, F. A., de Paula, A. A., Sousa, M. D., Cavalieri, A. V., & Kleine, V. G., “Lift enhancement by wavy leading edges at Reynolds numbers between 700,000 and 3,000,000”, 2018 Applied Aerodynamics Conference, AIAA 2018-3816, June 2018. https://doi.org/10.2514/6.2018-3816

[7] Chen, J. H., Li, S. S., & Nguyen, V. T., “The effect of leading edge protuberances on the performance of small aspect ratio foils”, 15th International Symposium on Flow Visualization, 2012, pp. 25-28.

[8] Hansen, K. L., Kelso, R. M., and Dally, B. B., “Performance Variations of Leading-Edge Tubercles for Distinct Airfoil Profiles,” AIAA Journal, Vol. 49, No. 1, 2011, pp. 185–194. doi:10.2514/1.J050631

[9] Rostamzadeh, N., Hansen, K. L., Kelso, R. M., and Dally, B. B., “The Formation Mechanism and Impact of Streamwise Vortices on NACA 0021 Airfoil’s Performance with Undulating Leading Edge Modification,” Physics of Fluids, Vol. 26, No. 10, 2014, Paper 107101. doi:10.1063/1.4896748

[10] Pedro, H. T. C., and Kobayashi, M. H., “Numerical Study of Stall Delay on Humpback Whale Flippers,” 46th AIAA Aerospace Sciences Meeting and Exhibit, AIAA Paper 2008-0584, Jan. 2008. doi:10.2514/6.2008-584

[11] Miklosovic, D. S., Howle, L. E., Murray, M. M., and Fish, F. E., “Leading-Edge Tubercles Delay Stall on Humpback Whale (Megaptera Novaeangliae) Flippers,” Physics of Fluids, Vol. 16, No. 5, 2004, pp. L39–L42. doi:10.1063/1.1688341

[12] Weber, P. W., Howle, L. E., Murray, M. M., and Miklosovic, D. S., “Computational Evaluation of the Performance of Lifting Surfaces with Leading-Edge Protuberances,” Journal of Aircraft, Vol. 48, No. 2, 2011, pp. 591–600. doi:10.2514/1.C031163

[13] Custodio, D., “The Effect of Humpback Whale-like Leading Edge Protuberances on Hydrofoil Performance,” M.S. Thesis, Mechanical Engineering Dept., Worcester Polytechnic Inst., Worcester, MA, 2007.

[14] Isaac, K., & Swanson, T., “Biologically inspired wing leading edge for enhanced wind turbine and aircraft performance”, 6th AIAA Theoretical Fluid Mechanics Conference, AIAA 2011-3533, June 2011. https://doi.org/10.2514/6.2011-3533

[15] Butt, F.R., and Talha, T., "A Numerical Investigation of the Effect of Leading-Edge Tubercles on Propeller Performance," Journal of Aircraft, Vol. 56, No. 3, 2019, pp. 1014-1028. doi.org/10.2514/1.C034845

[16] Ibrahim, I. H., and New, T. H., “A Numerical Study on the Effects of Leading-Edge Modifications upon Propeller Flow Characteristics,” Proceedings of the 9th International Symposium on Turbulence and Shear Flow Phenomena, TSFP-9 P-21, Melbourne, Australia, July 2015.

[17] Asghar, A., Perez, R. E., & Allan, W. D., “Further Parametric Investigation of Leading Edge Tubercles on the Propeller Performance”, AIAA Scitech 2019 Forum, AIAA 2019-0850, January 2019. https://doi.org/10.2514/6.2019-0850

[18] Zhe, N., and Hu, H., “An Experimental Study on the Aerodynamics and Aeroacoustic Characteristics of Small Propellers of UAV,” 54th AIAA Aerospace Sciences Meeting, AIAA 2016-1785, January 2016.
doi:10.2514/6.2016-1785
[19] Shi, W., Atlar, M., Norman, R., Day, S., & Aktas, B., “Effect of waves on the leading-edge undulated tidal turbines,” Renewable energy, Volume 131, 2019, pp. 435-447.
https://doi.org/10.1016/j.renene.2018.07.072
[20] Giada Abate and Dimitri N. Mavris, "CFD Analysis of Leading Edge Tubercle Effects on Wind Turbine Performance," 15th International Energy Conversion Engineering Conference, AIAA 2017-4626, July 2017.
https://doi.org/10.2514/6.2017-4626
[21] Giada Abate and Dimitri N. Mavris, "Performance Analysis of Different Positions of Leading Edge Tubercles on a Wind Turbine Blade," 2018 Wind Energy Symposium, AIAA 2018-1494, Jan. 2018.
doi.org/10.2514/6.2018-1494
[22] Shi,W., Atlar, M., Norman, R., Aktas, B., and Turkmen, S., “Numerical Optimization and Experimental Validation for a Tidal Turbine Blade with Leading-Edge Tubercles,” Renewable Energy, Vol. 96, Part A, 2016, pp. 42–55.
doi:10.1016/j.renene.2016.04.064
[23] Ri-Kui Zhang and Jie-Zhi Wu, “Aerodynamic characteristics of wind turbine blades with a sinusoidal leading edge,” Wind Energy, Vol. 15, No. 3, 2012, pp 407-424.
doi.org/10.1002/we.479
[24] Florian Krömer, Felix Czwielong and Stefan Becker, “Experimental investigation of the sound emission of skewed axial fans with leading-edge serrations,” 25th AIAA/CEAS Aeroacoustics Conference, AIAA 2019-2735, May 2019.
doi.org/10.2514/6.2019-2735
[25] Tu Baofeng, Zhang Kai, Hu Jun, “Investigation on Performance of Compressor Cascade with Tubercle Leading Edge Blade,” International Journal of Turbo & Jet-Engines, August 2019 (Ahead of print).
doi.org/10.1515/tjj-2019-0023
[26] Flow Simulation Technical Reference, 1st ed., Mentor Graphics Corp., Wilsonville, OR, 2018, pp. 4, 81.
[27] Taisuke Nambu, Atsushi Hashimoto, Takashi Aoyama, and Tetsuya Sato, “Numerical Analysis of the ONERA-M6 Wing with Wind Tunnel Wall Interference,” The Japan Society for Aeronautical and Space Sciences, Vol. 58, No. 1, 2015, pp 7-14.
https://doi.org/10.2322/tjsass.58.7
[28] Durrani, N., & Qin, N., “Comparison of RANS, DES and DDES results for ONERA M-6 Wing at transonic flow speed using an in-house parallel code,” 49th AIAA Aerospace Sciences Meeting including the New Horizons Forum and Aerospace Exposition, January AIAA 2011-190.
https://doi.org/10.2514/6.2011-190